Challenges and Perspectives for Lowering the Vertical-Component Long-Period Detection Level

Thomas Forbriger*[1], Walter Zürn[1], and Rudolf Widmer-Schnidrig[2]

Abstract

For observations of vertical-component acceleration in the normal-mode band (0.3–10 mHz), the detection sensitivity for signals from the Earth's body can be improved to levels below the Peterson low-noise model (PLNM). This is achieved by deterministic procedures that (at least partly) remove the accelerations originating from atmospheric mass fluctuations. The physical models used in such corrections are still too simple and fail at frequencies above 3 mHz. Anticipating improved atmospheric correction procedures, we explore the prospects of lowering the detection level. From recordings of excellent vertical-component sensors operated under exceptional site conditions at the Black Forest Observatory, we select time windows of very low background signal, for which all of the contributing broadband seismometers showed their best performance. Streckeisen seismometers of type STS-1, STS-2, and STS-6A, a Nanometrics Trillium T360, and the superconducting gravimeter (SG) SG056 manufactured by GWR Instruments take part in this comparison. Because of their low level of self-noise, the STS-1 and the SG056-G1 benefit the most from a correction with the best currently available improved Bouguer plate model for atmospherically induced signals at frequencies below 1 mHz. As far as we know, this is the first case in which the background level of a broadband seismometer could be lowered below the PLNM. At signal periods beyond the normal-mode band (investigated up to 12 hr), the gravimeters show the lowest level of self-noise, directly followed by the STS-6A. In the band from 0.3 to 10 mHz, the STS-1 has the lowest level of self-noise, which is at least 4 dB below the PLNM, directly followed by the T360 and the STS-6A. Sensors of lower self-noise than the currently manufactured STS-6A or T360 are needed before improved atmospheric correction procedures lead to a significantly lower vertical-component detection threshold.

Cite this article as Forbriger, T., W. Zürn, and R. Widmer-Schnidrig (2021). Challenges and Perspectives for Lowering the Vertical-Component Long-Period Detection Level, *Seismol. Res. Lett.* **92**, 2498–2512, doi: 10.1785/0220200399.

Supplemental Material

Introduction

Why does it matter?

There are several good reasons to strive for the detection of small amplitude signals at frequencies of 1 mHz and below. (1) Observations of the Earth's normal modes at very low frequencies, and analyses of their splitting and coupling provide unique constraints on deep structure (including anisotropy). Not all of them have yet been identified in observations (Laske and Widmer-Schnidrig 2015, their fig. 16). With improved signal-to-noise ratio (SNR), these observations may contribute to improvements of models of 1D and 3D structure, and dynamics of the Earth's core as pointed out by Widmer-Schnidrig (2003). (2) Because of the sensitivity of the low-frequency modes to 1D and 3D density structure, their observation at higher SNR will help to resolve the density structure independently from bulk and shear moduli (Häfner and Widmer-Schnidrig, 2013) and, thus, help to better understand the driving mechanisms of mantle (and core) convection. (3) Models of the large-scale anelastic structure of the mantle could benefit from enhanced SNR in observations of the attenuation of normal modes. Amplitude measurements suffer much more than frequency determinations from poor SNRs. Viscoelastic properties of the mantle are of vital importance for mantle convection and plate tectonics (Romanowicz and Mitchell, 2007). (4) Long-period observations are essential for a better understanding of the mechanisms of very deep earthquakes (Houston, 2007). (5) The *W*-phase, first described by Kanamori (1993), is promoted by Kanamori and Rivera

1. Geophysical Institute (GPI), Karlsruhe Institute of Technology (KIT), Black Forest Observatory (BFO), Wolfach, Germany; 2. Institute of Geodesy, University of Stuttgart, Black Forest Observatory (BFO), Wolfach, Germany

*Corresponding author: Thomas.Forbriger@kit.edu

(2008) and Duputel *et al.* (2012), for a rapid determination of the source mechanism and magnitude of megathrust earthquakes, and is composed of signals in the normal-mode band. (6) The so-called "prompt elasto-gravity signals" from seismic sources can be detected before the arrival of the *P* wave, and have been observed and modeled by Juhel *et al.* (2018) and Zhang *et al.* (2020) for very large magnitude quakes. Because of the emergent waveforms of these signals, only instruments with low levels of noise at very long periods are capable of unambiguous observation and can help to extend the observability to smaller magnitude earthquakes. (7) The background free spheroidal oscillations of the Earth (the so-called "hum"), first proposed by Benioff *et al.* (1959), are clearly observed between 2 and 7 mHz in vertical-component data (Kobayashi and Nishida, 1998; Nawa *et al.*, 1998; Suda *et al.*, 1998) and are, as well, present in horizontal-component recordings (Kurrle and Widmer-Schnidrig, 2008). Because the Earth is also a resonant physical system below 2 mHz, at some level, there should be background oscillations down to the gravest elasto-gravitational normal mode ($_0S_2$ near 0.3 mHz), whatever the driving mechanism is. Presently, the steep rise of the noise level below 2 mHz prevents this observation. (8) The so-called Slichter–Triplet (Slichter, 1961a,b), three translational modes of the inner core, should exist due to accepted physics, but have never been observed. If observed, their parameters (eigenfrequency, splitting, attenuation, and amplitudes) would provide unique information on the Earth's structure near the inner–outer core boundary (Smith, 1976; Rosat *et al.*, 2003; Rosat and Rogister, 2012). The amplitude of the signal, however, is estimated to remain far below present detectability thresholds. This is the case for the excitation by sporadically occurring megaquakes (Rosat, 2007) as well as for continuous excitation by outer core turbulence, as suggested by Busse (1974). (9) So-called core undertones (Crossley and Rochester, 1980) are also expected at very low frequencies, to provide signals. These are more speculative than the Slichter modes. Two types of waves in the liquid outer core, gravity waves on interfaces, and a kind of Rossby waves with the Coriolis force as a major part of the dynamics, could cause observable effects at the surface, given their amplitude is large enough and observation techniques are sensitive enough.

Where is the problem?

Observations in the frequency band of elasto-gravitational free oscillations of the Earth are particularly challenging. This is because with decreasing frequency the amplitude of the signal components carrying the desired information become small compared with other signal components (which include instrumental self-noise and local disturbances due to atmospheric attraction and loading). For this reason, instruments must be carefully shielded against thermal fluctuations and changes of air pressure (Forbriger, 2012). As the case may be, magnetic field-induced noise must be considered as well, like demonstrated by Forbriger *et al.* (2010) and recently discussed by Tape *et al.* (2020) and Díaz *et al.* (2020). The major issues remaining after all efforts of shielding and optimized coupling are the consequences of mass fluctuation in the atmosphere and, of course, instrumental self-noise of the sensor.

To provide observations with lower noise floor, not only valid correction models for signals induced by atmospheric mass fluctuation must be improved, but also the seismic instruments themselves must be capable to properly measure signals at this level.

Where are the current limits?

Low-noise models. Low-noise models are commonly taken both as a reference and to set the design goals for sensitive broadband seismometers. At frequencies below about 3 mHz, they, however, do not represent the signal level produced by vibrations of the Earth's body. Rather, they specify the lower envelope curve for a certain data set, under a certain statistical evaluation (which might be different for each model), and provide an estimate of the floor level of the background signal for this data, but no more.

At frequencies below 3 mHz, the background noise level of seismic observations, in terms of acceleration power spectral density (PSD), typically increases with decreasing frequency. This is demonstrated by standard low-noise models. A classic and still frequently used model for the Global Seismographic Network (GSN) was published by Peterson (1993). He calls this model "new low-noise model" to distinguish it from an older one. We refer to his model as the Peterson low-noise model (PLNM). The GSN noise model by Berger *et al.* (2004) is a more recent analysis. Both use different approaches of statistical analysis. Anthony *et al.* (2020) discuss how this may result in slightly different levels for the final model curves. When comparing these curves to PSD, as computed for seismometer recordings, we shall keep in mind that the low-noise models do not represent a single recording but a lower envelope (PLNM) or the 1st percentile (GSN noise model) for a large collection of data. In the current study, we use the PLNM just as a reference level in diagrams, which display the analysis results for specific recordings.

In any case, low-noise models represent the lowest background signal level, whatever the cause. At or below this level, there exist signals containing valuable information on Earth structure and dynamics. The background free oscillations set the level from 2 to about 10 mHz (Berger *et al.*, 2004, their fig. 8). At frequencies below 1 mHz, seismic sensors of most types, obviously, are limited by self-noise, as a comparison by Berger *et al.* (2004, their fig. 9) shows. The signal levels presented in the PLNM as well as in the GSN noise model, at frequencies below 1 mHz, represent the smallest level observed with STS-1 vertical-component seismometers. Whether this represents instrumental self-noise or the effect of fluctuations of masses in the atmosphere is under discussion. We investigate this in the current study.

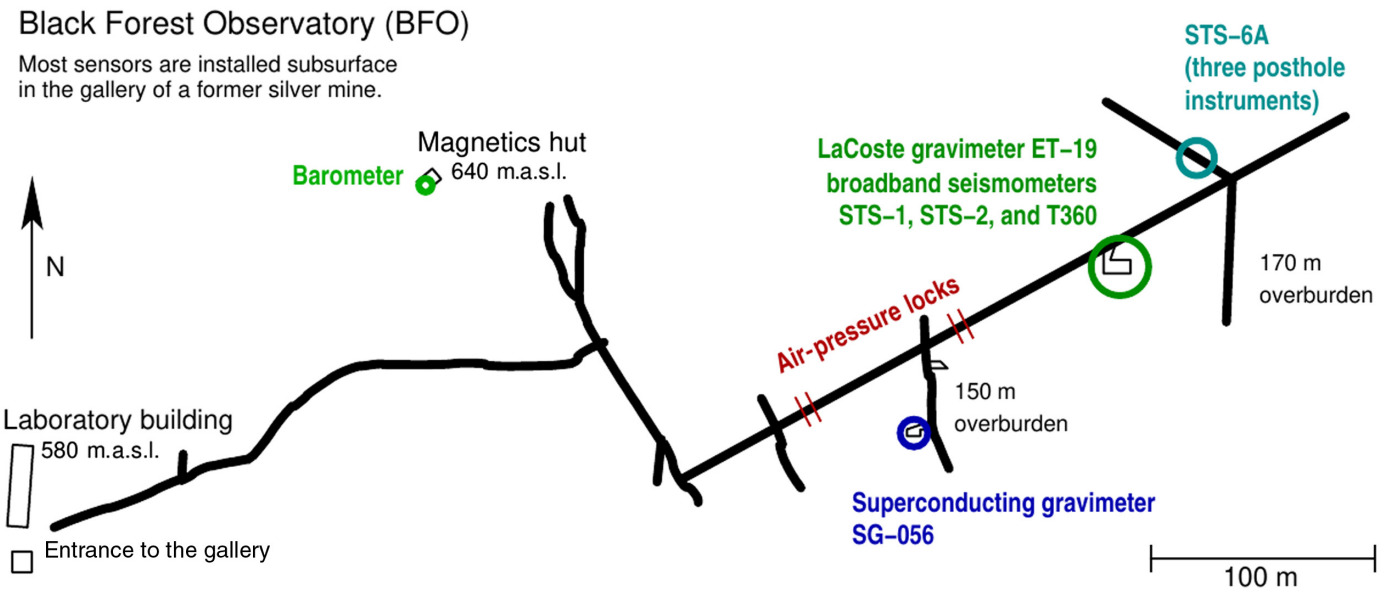

Figure 1. Floor map of the Black Forest Observatory (BFO). The instruments are installed in a former silver mine. The gallery leads gently up into the granitic rock of a hill. The vault of the superconducting gravimeter (SG; with sensors SG056-G1 and SG056-G2) is located behind the first air lock. The seismometers (STS-1, STS-2, T 360, and STS-6A) are additionally protected by a second air lock. The thickness of overburden increases from a few meters at the entrance to about 150 m at the SG and 170 m at the STS-6A. The barometer (Paro6016B) is located at the surface in a hut, about 60 m above the gallery. The color version of this figure is available only in the electronic edition.

Anyhow, the low-noise models do not represent the noise floor originating from the Earth's body, at frequencies below 1 mHz. Zürn and Widmer (1995, their fig. 1) demonstrate this by a partial correction for disturbances originating from the atmosphere as well as Rosat and Hinderer (2011, their fig. 1) do in an analysis of recordings from superconducting gravimeters (SGs). At frequencies below 1 mHz, the presented levels tend to be below the PLNM.

Environmental sources of noise. To resolve signals at the level of the PLNM, at frequencies in the normal-mode band (0.3–10 mHz) and below, the instruments must be operated in a very low noise environment. In particular, temperature, air pressure in the vault, and magnetic field must be kept stable. The levels of fluctuations, which must not be exceeded, are challengingly low (Forbriger, 2012, his section 5.1: less than 10^{-6} K for temperature and less than 10^{-5} hPa for air pressure at the minimum of the noise floor near 3 mHz). Nevertheless, seismometers can be effectively shielded against these environmental conditions. It is, however, impossible to shield against Newtonian attraction caused by atmospheric masses and water fluctuations in the hydrosphere. Crossley *et al.* (2013, their fig. 2) point out that the Slichter Triplet and core modes are still hidden below the level of noise originating from environmental sources at frequencies below 1 mHz.

Models of noise caused by fluctuations of atmospheric mass. For the impact of atmospheric mass fluctuations, considerable research has been done, which resulted in models linking local atmospheric pressure to recorded vertical acceleration. Zürn and Widmer (1995, their fig. 1) demonstrate the effectiveness of a frequency-independent correction on seismometer data. At the time, this type of correction was already common in tidal analysis of gravimeter data (Warburton and Goodkind, 1977; Merriam, 1992; Crossley *et al.*, 1995). For the LaCoste-type gravimeter earth-tide (ET)-19 at Black Forest Observatory (BFO) Zürn and Widmer (1995, their fig. 2) demonstrate the ability to lower the detection threshold even below the PLNM, for frequencies below 1.5 mHz.

The mechanisms by which the atmosphere acts on the seismic sensor often are expressed in terms of an admittance $\alpha(f)$ (possibly depending on frequency f) by which the change of locally recorded air pressure $\Delta p(f)$ appears in the record of acceleration $\Delta g(f)$. The currently most advanced model for local admittance proposed by Zürn and Wielandt (2007, their equation 4) is called the improved Bouguer plate model (IBPM). It accounts for (1) the direct Newtonian attraction of atmospheric masses, (2) the change in gravity to which the sensor is exposed due to its vertical motion, when the Earth's crust is depressed by the atmospheric surface load, as well as (3) the inertial acceleration of the seismometer going along with this. This model is frequency dependent, due to the consideration of inertia. The three contributions cancel near 3 mHz, in which the exact notch frequency depends on the elastic properties of the crust. This model, hence, predicts an absence of atmospherically induced noise in a narrow frequency band near 3 mHz. It proves applicable in many cases; however, is still too simple in that it (1) inherently assumes

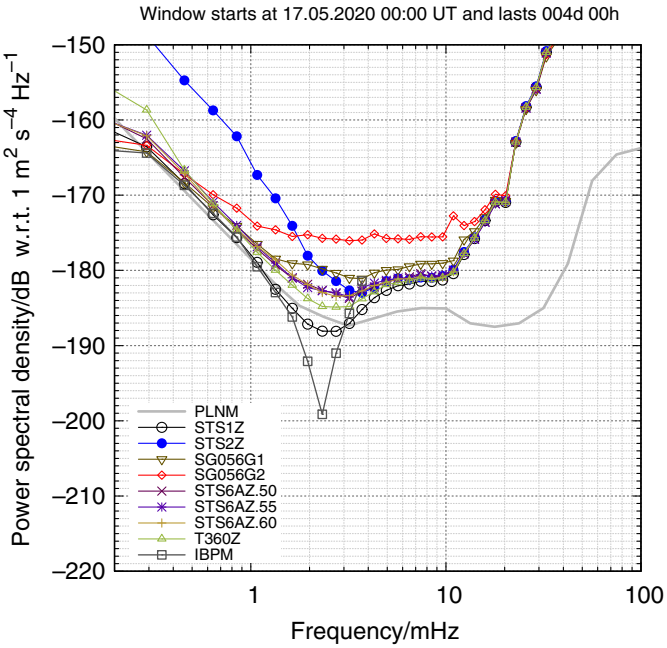

Figure 2. Power spectral density (PSD) computed for the signal recorded by eight vertical-component sensors in the time of four days, beginning at 17 May 2020 00:00 UT. PSD is displayed in decibel referred to corresponding ground acceleration with 1 $m^2\,s^{-4}\,Hz^{-1}$. The Peterson low-noise model (PLNM; Peterson 1993) is displayed as a reference level by the thick solid gray line. The signals are taken from vertical components of the instruments listed in Table 1. The signal level displayed by a solid gray line with open squares is computed from a local recording of air pressure (barometer: Paro6016B in Table 1) by application of the improved Bouguer plate model (IBPM; Zürn and Wielandt 2007). It represents the expected contribution due to mass fluctuations in the local atmosphere. This curve is truncated at 4 mHz, because the effect is unrealistically overpredicted at higher frequency by the simple model. The color version of this figure is available only in the electronic edition.

a stratified layering of atmospheric masses and in that it (2) neglects the inertial response of the crust to the loading force. These shortcomings let the model overpredict the induced signal at frequencies above the minimum of the admittance (i.e., above 3 mHz). Nevertheless, Zürn and Meurers (2009) could demonstrate that the observed admittance changes its sign near 3 mHz, like predicted by the model. A corresponding minimum at 3 mHz is present in the global low-noise models (Peterson, 1993; Berger *et al.*, 2004), as pointed out by Zürn and Wielandt (2007).

We make use of a slightly modified IBPM-model, to investigate the composition of the noise floor of the instruments under investigation. For this reason, a few introductory remarks seem appropriate. The admittance function

$$\alpha(f) = \frac{\Delta g(f)}{\Delta p(f)} = -\frac{2\pi G}{g_0} + \frac{D}{\lambda + 2\mu}\left(4\pi^2 f^2 + \left|\frac{\delta g}{\delta z}\right|\right), \tag{1}$$

as given by Zürn and Wielandt (2007, their equation 4) relates the recorded change in vertical acceleration expressed as a change in gravity $\Delta g = \alpha \Delta p$ to a change in local air pressure Δp. The term $-2\pi G\, g_0^{-1}$ expresses the Newtonian attraction of a stratified atmosphere, for which $G = 6.673 \times 10^{-11}$ $Nm^2\,kg^{-2}$ is the gravitational constant and $g_0 = 9.81$ $m\,s^{-2}$ is gravity. The effective admittance is reduced by the fact that the Earth's crust is deformed by the surface loading of the atmosphere, which results in a vertical displacement of the sensor in the Earth's heterogeneous gravity field. The model accounts for this by a homogeneous elastic layer of thickness D on a rigid substratum. If the compressional wave modulus of the layer is $\lambda + 2\mu$, with the shear modulus μ and λ being Lamé's constant, vertical subsidence

$$\Delta z = \frac{D}{\lambda + 2\mu}\Delta p, \tag{2}$$

results from an increase Δp of air-pressure. In equation (1), $|\delta g \delta z^{-1}| = 3.08 \times 10^{-6}$ s^{-2} is the free-air gradient of gravity, and, f^2 results from inertial acceleration, with f being signal frequency.

A characteristic parameter is the zero frequency (DC)-admittance

$$\alpha_{DC} = \alpha(f = 0) = -\frac{2\pi G}{g_0} + \frac{D}{\lambda + 2\mu}\left|\frac{\delta g}{\delta z}\right|, \tag{3}$$

the asymptotic value at lower frequency. At the lower limit of the frequency band of investigation (0.2 mHz in our case) in many cases, we find α to be near −3.5 $nm\,s^{-2}\,hPa^{-1}$. The second characteristic parameter is the notch frequency

$$f_n = \frac{\sqrt{\frac{2\pi G}{g_0}\frac{\lambda+2\mu}{D} - \left|\frac{\delta g}{\delta z}\right|}}{2\pi}, \tag{4}$$

which is near 3 mHz, as indicated by the low-noise models. The model in equation (1) has only one free parameter, namely the elasticity of the layer expressed by the factor $D\,(\lambda + 2\mu)^{-1}$. A layer with a DC-admittance near −3.5 $nm\,s^{-2}\,hPa^{-1}$ would have a notch frequency of 0.594 mHz and for a notch frequency near 3 mHz the DC-admittance would be close to the pure gravitational effect $-2\pi G g_0^{-1} = -4.27$ $nm\,s^{-2}\,hPa^{-1}$. The model is clearly oversimplified, and, indications for that are also seen in the data, as discussed subsequently. With the available data, we currently see no point in developing a more elaborate model. However, to allow the model to satisfy the two characteristic parameters, DC-admittance and notch frequency at once, we parameterize the model by

$$\alpha(f) = \frac{\Delta g(f)}{\Delta p(f)} = \alpha_{DC}\left(1 - \frac{f^2}{f_n^2}\right), \tag{5}$$

such that both parameters can be set independently. Values for the DC-admittance, α_{DC}, and the notch frequency, f_n, are then adjusted by fitting the model predicted signal to the observed vertical acceleration record. The optimal values typically vary

with time window and frequency band, which is another indication of the oversimplification of this model. Equation (5) is identical with equation (1), if equations (3) and (4) are satisfied.

What do we contribute here?

We use signals from nine vertical-component instruments operated at BFO (1971), to analyze the composition of the noise floor of observations made in the normal-mode band (0.3–10 mHz). We limit this study to vertical-component sensors, because horizontal components, additionally, experience tilt-coupled gravity (Wielandt, 2012, his section 5.3.3) and, therefore, typically show a higher level of background signal at frequencies below 10 mHz, as demonstrated by Berger *et al.* (2004, their fig. 7). A discussion of horizontal components, therefore, would, additionally, have to address coupling to bedrock, horizontal gradients of surface loading, cavity effects, and other issues, like discussed by Zürn *et al.* (2007).

Tilt-coupled gravity is a first-order effect in the horizontal component and a second-order effect in the vertical component, which is obvious when decomposing the gravity vector into the components of the tilted seismometer. Thus, if the level of the 1st percentile of the horizontal-component GSN noise model (Berger *et al.*, 2004) would be controlled by tilt-coupled gravity (which we assume), then the same signal would contribute to the noise level of the vertical component at 200 dB below the level of the PLNM. Conversely, because tilt-coupled noise is of second order in the vertical component, tilt-coupled gravity that would exceed the level of the PLNM in the vertical component would produce a background level in the horizontal component about 100 dB above the GSN noise model. This is not what we see. For this reason, we have evidence that tilt-coupled gravity does not contribute to the vertical-component noise floor.

For the vertical component, we discuss the prospects of the application of current deterministic models of noise induced by the atmosphere and required improvements for them. Furthermore, we investigate the level of self-noise observed at the most capable broadband vertical-component seismometers currently available in deployments of the GSN. For instruments with a homogeneous triaxial Galperin-type arrangement of oblique internal sensors (Wielandt, 2012, his section 5.3.7), the level of self-noise of the vertical component is controlled by all three internal sensors, and such is also a measure for the instrumental self-noise expected in the horizontal-component data.

Observations

Sensors and data

An essential prerequisite to detect small-amplitude signals from the Earth's interior, at long signal periods, is proper shielding against local disturbances acting on the sensors. For vertical-component inertial seismometers, the most prominent of such disturbances result from thermal fluctuations and changes in ambient air pressure. Seismic instruments are sensitive to these environmental conditions, due to finite temperature coefficients of their components, deformation of their casing, or buoyancy acting on the probe mass (if not properly shielded). For this reason subsurface installations are mandatory. At BFO, air locks, additionally, shield the instruments against fluctuations of ambient pressure and prevent convective heat exchange with the exterior. Zürn and Wielandt (2007) and Forbriger *et al.* (2010) describe the shielding provided at BFO, which makes this observatory one of the most suitable places for the observation of the Earth's normal modes on the globe. An extensive overview of research done under these favorable conditions is provided by Zürn (2014).

TABLE 1
Instruments Used in This Study

Sensor	Serial Number	Net	Station	Loc	Chan
STS-1	SN 28740	II	BFO	00	LHZ
STS-2	SN 19123	GR	BFO		LHZ
STS-6A	SN 176254	II	XBFO	50	LHZ
STS-6A	SN 150804	II	XBFO	55	LHZ
STS-6A	SN 176241	II	XBFO	60	LHZ
T 360	SN 0052	II	XBFO	70	LHZ
SG056-G1	SN 056	II	BFO	00	LG1
SG056-G2	SN 056	II	BFO	00	LG2
ET-19	SN 19	II	BFO	00	LGZ
Paro6016B	SN 90720	II	BFO	10	LDO

Instruments are identified by the sensor type and serial number. The data source (Black Forest Observatory [BFO], 1971) is specified by the SEED network code (Net), station code (Station), location code (Loc), and channel code (Chan). Metadata can be obtained from the IRIS MetaData Aggregator (see Data and Resources), based on these SEED codes. Results for ET-19 are shown only in the supplemental material (Fig. S10). Station code XBFO (experimental) is used for temporary deployments. ET-19, earth-tide 19; IRIS, Incorporated Research Institutions for Seismology; SEED, Standard for Exchange of Earthquake Data.

Figure 1 shows a map of the gallery. The instruments used in the current investigation are listed in Table 1. Signals are recorded with Quanterra Q330HR digitizers, with 26-bit resolution and preamplifiers being disabled in all cases. Data are available through the Data Management Center of the Incorporated Research Institutions for Seismology (network code II, Scripps Institution Of Oceanography, 1986) and (in case of the STS-2, network code GR) as a part of the German Regional Seismic Network through the Data Management Center at the Federal Institute for Geosciences and Natural Resources (BGR) (1976, Germany).

STS-1. The STS-1 broadband seismometer was developed by Wielandt and Streckeisen (1982). Its vertical-component

sensor uses a leaf-spring suspension (Wielandt, 1975). The approximate geometry of the leaf-spring and the pendulum is sketched by Wielandt (2012, his fig. 5.7a) and is reproduced by Aki and Richards (2002, their fig. 12.23) from Wielandt and Streckeisen (1982). The later very broadband version uses the same mechanical sensor but a feedback for an eigenperiod of 360 s (Wielandt and Steim, 1986). The invention of this instrument marks the advent of modern broadband seismology. It still sets the standard in the GSN, in terms of low self-noise at low frequency. Low-noise models (Peterson, 1993; Berger *et al.*, 2004), at low frequencies, mainly represent the signal level recorded with instruments of this type. Ringler and Hutt (2010, their fig. 11) provide a self-noise analysis for the STS-1.

The STS-1 has been out of production for more than a decade, and the manufacturer, Streckeisen, no longer provides support for maintenance of existing sensors. For this reason, the GSN urgently searches for a competitive replacement sensor for stations, where sensors of STS-1 type are irrecoverably damaged. Hafner *et al.* (2018) report the efforts to identify such sensors, after funding was made available by the National Science Foundation.

In comparison to the other broadband seismometers used in the current investigation, the STS-1 is unique in several respects: (1) A set consists of two dedicated horizontal sensors and one vertical sensor, existing as individual instruments. (2) The mechanical sensors are installed in a partially evacuated housing. (3) The feedback electronics is separate from the mechanical sensor, resulting in excess heat only marginally affecting the mechanical system. (4) The free period of the mechanical system, which controls the overall sensitivity together with the resolution of the displacement transducer, is adjusted manually, as a part of the setup procedure and typically is longer than what is achieved for other seismometers. (5) The instrument uses an inductive displacement transducer (linear variable differential transformer), which typically is less sensitive than the capacitive (three-plate capacitor) transducer used in the other instruments (Wielandt, 2012, his section 5.3.9). The first four have the potential to improve performance, whereas the fifth is expected to reduce sensitivity.

The STS-1Z, at BFO, is installed at the southern wall of the seismometer vault (Fig. 1).

STS-2. The Streckeisen STS-2 has the shortest eigenperiod (120 s) of the seismometers in the current comparison and is less sensitive in the normal-mode band by design. It contains a homogeneous, triaxial Galperin-type arrangement of three identical sensors that use leaf-spring suspensions. Wielandt (2012, his figs. 5.7b and 5.10) provides schematic sketches. Wielandt and Widmer-Schnidrig (2002) describe the instrument and provide a self-noise model for the standard version. Ringler and Hutt (2010, their fig. 12) provide a self-noise analysis for a high-gain version of the STS-2, with improved sensitivity in the Earth's normal-mode band.

Compared with the STS-1, the STS-2 provides some convenience and became very popular in the 1990s for this reason: (1) All three components are contained in a single compact casing, together with the feedback electronics. (2) The instrument benefits from the more sensitive capacitive displacement transducer. As a consequence, manual adjustment of the mechanical free period is not necessary (not even possible) during setup. (3) The balance of the mechanical sensor (torque due to suspension versus torque due to gravity) is adjusted automatically by electronic circuitry. (4) During adjustment the sensor is operated in a 1 s mode, thus avoiding the long (several minutes) transients in the response of the STS-1 to manual adjustment. (5) The sensor comes in an air-tight and warp-free casing. A vacuum pump, such as with the STS-1, is not needed. (6) This instrument has a significantly reduced power consumption (1.8 W for the STS-2, compared with almost 11 W for one set of STS-1s). All these benefits come at the cost of increased self-noise to some degree. Still, the STS-2 is an excellent and sensitive broadband seismometer.

The STS-2 at BFO is installed at the southern wall of the seismometer vault, next to the vertical component of the STS-1 (Fig. 1).

STS-6A. The Streckeisen STS-6A is one of the sensors selected by IRIS, as a replacement for primary sensors in the GSN (Hafner *et al.*, 2018). It is designed to meet the latest requirements set by the U.S. Geological Survey (USGS). The STS-6A is a borehole instrument by design and the only instrument of this form factor in the current comparison. It contains a homogeneous, triaxial Galperin-type arrangement of three identical sensors that use leaf-spring suspensions. In the huddle test at BFO, we operate three of these sensors in about 160 cm deep boreholes drilled (through a concrete pier) into the rock of the floor of the mine. The installation follows the recommendations by the Albuquerque Seismological Laboratory (USGS), which includes a stainless steel pipe of 17.5 cm in diameter with closed bottom to separate the sensor from the water, which unavoidably accumulates in the borehole. All three sensors are installed, approximately, along the symmetry axis of the gallery, with 50 cm spacing between boreholes. Their location is shown in Figure 1.

T360. The Nanometrics Trillium T360 is another one of the sensors selected by IRIS, as a replacement for primary sensors in the GSN (Hafner *et al.*, 2018). The instrument is provided by the manufacturer in three different casings, alternatively. This comprises a traditional vault sensor, a posthole sensor, and a borehole sensor. It contains a homogeneous, triaxial Galperin-type arrangement of three identical sensors that use leaf-spring suspensions. The instrument in the current investigation is a vault sensor, which was installed on a pier next to the STS-2 at the southern wall of the seismometer vault (Fig. 1). The cover

supplied together with the instrument was used for thermal insulation, as recommended by Nanometrics.

SG056-G1 and SG056-G2. SGs are the current standard for the observation of tidal and secular gravity changes. Instruments of this type typically provide a drift rate smaller by up to a factor of 1000, with respect to the drift observed with the best spring-type gravimeters. The only manufacturer for commercial instruments of this design, currently, is GWR instruments at San Diego (U.S.A.). SGs were developed as early as the 1960s (Prothero and Goodkind, 1968). In the 1990s, they were still challenged by spring gravimeters (Richter *et al.*, 1995) but were significantly improved since then. Goodkind (1999) and Hinderer *et al.* (2007) describe this type of instrument and developments involved. Widmer-Schnidrig (2003) points to the potential of these instruments in application to normal-mode research.

The SG056 operates, since 2009, at BFO (Fig. 1). Forbriger and Heck (2018, their section 2) describe this particular instrument. It is a so-called dual-sphere observatory SG and contains two sensors in a single package within a common dewar. The sensor SG056-G1 is special in that it has a larger probe mass of 17.7 g, whereas SG056-G2 has the standard mass of 4.34 g. SG056-G1 is the lower sensor in the package and, for this reason, potentially is better shielded against ambient conditions (magnetic field, in particular). Rosat and Hinderer (2011) conclude that SG056-G1 provides an exceptionally low noise level in the normal-mode band in a comparison of SGs in the data base of the International Geodynamics and Earth Tide Service (Voigt *et al.*, 2016).

ET-19. The ET-19 is a spring-type gravimeter, using the suspension invented by LaCoste (1934). It is instrument number 19 in the ET series manufactured by LaCoste. Ness *et al.* (1961) reported the first observation of normal modes, made with instrument number 4 after the Chilean earthquake of May 1960. Afterward, the mechanical feedback of these instruments was replaced by an electrostatic one, because of nonlinearities in the mechanics (Weber and Larson, 1966). The success of these instruments encouraged the project IDA to use LaCoste gravimeters (of a slightly less sophisticated type than the ET series) for their first deployment (Agnew *et al.*, 1986). They provided the first globally distributed network observations of normal modes. ET-19, for more than two decades, challenged other instruments with normal-mode recordings of exceptional quality. Unfortunately, it got damaged by a lightning surge, and lost its air-tightness and never fully recovered from this. We show an analysis of the noise floor in the supplemental material only (Fig. S10), because, the instrument could not compete with the others in May 2020, due to a nonlinear response to the short-period surface waves generated by the M_w 5.7 earthquake at 18 May 2020 23:22:34 UTC near Crete. The integral (only) electrostatic feedback of the instrument loses control of the pendulum in such cases.

Paro6016B. As a consequence of research reported by Zürn and Widmer (1995), which made the effect of atmospheric mass fluctuation in long-period and tidal records obvious, barometers nowadays usually are collocated with gravimeters and long-period seismometers. At BFO, we operate several barometers at the surface as well as behind the air locks. In the current study, we use a digital barometer model 6000-16B produced by Paroscientific. It is installed at the surface, in a separate building, as shown in Figure 1. Schaad (2016, his fig. 7) reports a noise floor for this type of instrument for which PSD increases with decreasing frequency in the millihertz range. At 1 mHz, the PSD of the incoherent signal component is about 5×10^{-7} $\mathrm{hPa^2\,Hz^{-1}}$. With the standard frequency-independent admittance of -3.5 $\mathrm{nm\,s^{-2}\,hPa^{-1}}$ for atmospheric effects, this would result in a level of 6×10^{-6} $\mathrm{nm^2 s^{-4}\,Hz^{-1}}$, which is at about -230 dB with respect to 1 $\mathrm{m^2 s^{-4}\,Hz^{-1}}$. Self-noise of the barometer, hence, does not compromise the validity of the conclusions drawn later. Barometers of the class of the Paro6016B make use of a correction procedure, to reduce effective sensitivity for temperature variation. With the available data, we cannot estimate the level at which residual disturbances due to imperfect temperature correction would compromise the pressure data. This level definitely is below the level of signals discussed here, but, it should be reconsidered, once seismometer self-noise and improved models for atmospheric effects allow a correction of seismometer data to lower levels.

Signal levels

We select a time window in 2020, which lasts from 17 May 00:00 UT to 21 May 00:00 UT. In this time window, only earthquakes of magnitudes smaller than M 6 occurred. They, practically, do not contribute to signals in the normal-mode band. At the same time, the local atmosphere is quiet and produces only a minor contribution to the signal in the band of interest. In the supplemental material, we show additional results for a time window in January 2019.

Figure 2 shows PSD of signals recorded with the instruments in this study, during the four day time period mentioned earlier. We average 100 segments for each time series, for which segments are overlapping by 50%. The obtained values of one-sided PSD (i.e., twice the Fourier transform of the autocovariance function, see Blackman and Tukey, 1958) are averaged over 1/20 decade. Harmonics at tidal frequencies of Q1, O1, K1, N2, M2, S2, and M3 were removed prior to spectral analysis. These are all outside the investigated frequency band but could affect the results through spectral leakage due to the large amplitude of these harmonics, in particular, in the gravimeter data. Instrument output level is compared with the PLNM (Peterson, 1993) and the signal level expected due to mass fluctuation in the local atmosphere (curve IBPM in

Fig. 2), if the IBPM-model (Zürn and Wielandt, 2007) is applied to a recording of local air pressure (Paro6016B in Table 1).

Signal levels are consistent at larger values of frequency (>20 mHz) where acceleration due to ground-motion dominates, such that all instruments record the same signal. A magnitude 5.7 earthquake in Crete (Greece) on 18 May 23:22 UT dominates the signal level in this frequency band. All curves coalesce at low frequency (<1 mHz), except for the STS-2. At frequencies below 3 mHz, the latter typically produces a level of self-noise, about 10 dB (and more) above the PLNM, which is well represented in the GSN noise model (Berger *et al.*, 2004, their fig. 9). Ringler and Hutt (2010) report that the high-gain version of the STS-2 produces long-period noise at a lower level than seen here for the standard version. The fact that the curves including the predicted contribution by the atmosphere (curve IBPM in Fig. 2) coalesce indicates that the signal level at low frequency is controlled by the atmospheric mass fluctuations. The fact that this happens at the level of the PLNM may indicate that the PLNM itself might represent smallest contributions of the atmospheric mass fluctuations at frequencies below 1 mHz. This suggests that we should be able to reduce the signal level by subtracting the signal predicted by the IBPM-model from the seismometer recording in the time domain. We test this subsequently.

The minimum of the admittance predicted by the IBPM-model is obvious from the minimum of the corresponding signal level (curve IBPM in Fig. 2) near 2.3 mHz. Consistently, the level of background signal is reduced near this frequency, which corresponds with a minimum in the PLNM. The STS-1 and the T360 are able to detect the cancellation of different mechanisms through which the atmosphere contributes to the signal, for which the STS-1 clearly presents the smallest signal level of all instruments. The three sensors of STS-6A type, the SG056-G1, and the STS-2, show only a slight minimum in signal level in the frequency band between 2 and 5 mHz. At least, for the SG056-G1, the minimum is clearly shifted in frequency and, apparently, is not due to the cancellation of effects of atmospheric origin but rather represents the frequency characteristic of other signal components.

The upper sensor SG056-G2 of the SG presents a signal level larger than the level of most other sensors in the band from 0.6 to 20 mHz. This is discussed to possibly be a consequence of the smaller probe mass (4.34 g), which may result in a higher level of thermal noise when compared to the lower sensor (SG056-G1, 17.7 g). However, this is not yet confirmed by experiment. The signal level of the T360 is elevated with respect to the others, at frequencies below the band of the Earth's free oscillations (<0.3 mHz).

For other time windows of quiet atmosphere, low-earthquake activity, and absence of instrumental glitches, we find similar signal levels. See the example shown in Figure S5. The results follow a similar general characteristic, with differences of only a few decibels, which are not considered to be statistically significant.

Analysis of the noise floor

To investigate the composition of the noise floor for the different sensors, we apply a correction for signals induced by the atmosphere. This is just like the correction introduced by Zürn and Widmer (1995) but using the frequency-dependent IBPM-model. If the detection level, in fact, would be limited by signals caused by the atmosphere, the correction should result in lower PSD levels. We show that this is the case, indeed. By comparison with the observations, we adjust the two parameters of equation (5) to the DC-admittance $\alpha_{DC} = -3.5$ nm s^{-2} hPa^{-1} and the notch-frequency $f_n = 2.25$ mHz. We apply the correction in the time domain prior to computation of PSD. The very same correction time series is used for each of the investigated seismometers. Within the framework of a homogeneous elastic layer of granite ($\lambda = \mu = 25$ GPa) with rigid base, $\alpha_{DC} = -3.5$ nm s^{-2} hPa^{-1} would be obtained for thickness $D = 190$ km and $f_n = 2.25$ mHz for $D = 17$ km.

Further, we compute the signal level of the incoherent signal of each sensor, by application of a three-channel correlation analysis (TCCA, Sleeman *et al.*, 2006). The latter is understood as the level of instrumental self-noise. The available set of instruments allows us to choose various combinations of TCCA reference instruments in this analysis, which provides a welcome opportunity to check consistency. If a subset of the sensors should experience coherent disturbances, this will become obvious in a deviation of incoherent PSD in cases in which they are used as a reference. No correction for atmospheric effects is applied in this analysis, and levels of incoherent signal do not depend on the parameters of the IBPM-model for this reason.

The levels obtained from the instruments listed in Table 1 are compiled in Figure 3. Analysis results, with respect to additional reference sensors, are displayed in Figures 4–7 and in the supplemental material. Unstable results of the TCCA are commonly obtained in the band of marine microseisms, and are present in Figure 3 at 50 mHz and above, for which signal level rapidly rises with frequency (Fig. 2). This incoherent component is only a small fraction of the total signal and is a short-wavelength-phenomenon, apparently caused by slight misalignment of the sensors. We do not apply the correction proposed by Gerner *et al.* (2016), because these issues are located outside the frequency band of interest in the current study. The results are discussed in the following sections, in detail.

Part of the instrumental self-noise is contributed by digitizer noise. We estimate the level of the latter contribution. All signals (except air pressure) are recorded with Quanterra digitizers of type Q330HR, with 26-bit resolution. These digitizers are designed such that quantization noise sets the noise floor near the Nyquist frequency only. In the frequency band of investigation, the digitizer noise is dominated by noise with,

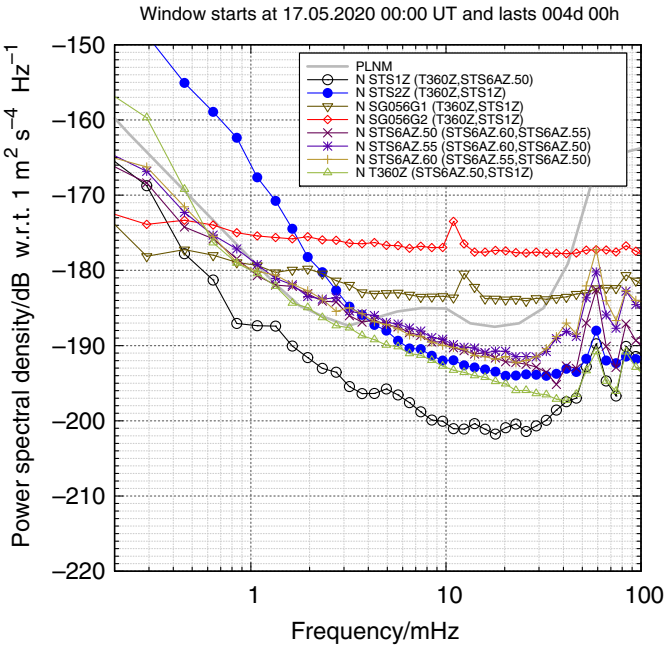

Figure 3. PSD of the incoherent component of the recorded signals for the time of four days, beginning at 17 May 2020 00:00 UT. The levels are computed by a three-channel correlation analysis (TCCA) for the signals recorded by eight vertical-component sensors with respect to two reference sensors each (given in parentheses in the legend). The signals are taken from vertical components of the instruments listed in Table 1. No correction with a model of atmospheric disturbance is involved. One-sided PSD is displayed in decibel referred to corresponding ground acceleration with 1 m^2s^{-4} Hz^{-1}. The PLNM (Peterson, 1993) is displayed as a reference level by the thick solid gray line. The color version of this figure is available only in the electronic edition.

approximately, a $1/f$-characteristic of PSD that originates in the electronic circuitry. We take this level as if it were the output of the sensors and compute corresponding values of recorded acceleration for comparison. In all cases, the level of incoherent signal is controlled by the seismometer alone, with no significant contribution from the digitizer.

To estimate the PSD of digitizer noise, we record the vertical-component output of an STS-2 on three inputs of the Q330HR SN 4409, simultaneously, and compute a TCCA to estimate the PSD of the incoherent signal component. This turns out to be identical with the PSD level of signals recorded with open unterminated inputs and to be about 15 dB below the manufacturers specification at 1 mHz (Kinemetrics, 2020). We compared recordings made in the extremely stable thermal environment of the mine, on the one hand, with recordings made in the laboratory with a peak-to-peak temperature variation of 6°C recorded internally by the Q330HR SN 4409 over 20 days, on the other hand. Temperature stability does not appear to be an additional benefit for the low-noise level of the Q330HR, which, in both cases, is observed to be lower than specified by the manufacturer.

Subsequently, we discuss the composition of background signal for the STS-1, SG056-G1, STS-6A, and T360. Results for the STS-2 (Fig. S1), the SG056-G2 (Fig. S2), and two of the STS-6As (Figs. S3 and S4) are shown in the supplemental material.

The STS-1. The results for the STS-1 are displayed in Figure 4. We focus on the signals in the normal-mode band below 10 mHz and truncate the frequency axis at 0.2 mHz. PSD values at lower frequencies are of questionable statistical significance, due to too few signal cycles being present in the time window.

At frequencies of 1 mHz and smaller, the PSD of the recorded signal (solid red line, open diamonds) and the PSD of the signal contribution predicted by the IBPM-model (solid gray line, open squares) align with the PLNM (thick solid gray line). That suggests that the recorded signal at these frequencies is dominated by the effect of atmospheric mass fluctuation and that, possibly, the PLNM reflects the signal level caused by the atmosphere during the quietest conditions. The difference of the seismometer signal and the IBPM-prediction should then be at a lower level of PSD, which, in fact, is the case for frequencies below 1 mHz (solid, dark red line, filled squares). The detection capability of the STS-1 in that frequency band, obviously, can be improved to below the level of the PLNM, by an appropriate correction for atmospherically induced signals. This is well known from the analysis of gravimeter data (Zürn and Widmer, 1995, their fig. 2), but is here reported for a seismometer for the first time. Although, the level predicted by the IBPM-model does not exceed the PSD of the output of the STS-1 up to 3 mHz, the difference of both signals is larger than the original output level for frequencies above 1.5 mHz. This clearly indicates that the IBPM-prediction does not match the actual recording at these frequencies. The limitation of the model becomes obvious at frequencies above 3 mHz, for which the inertial component of the IBPM-model strongly overpredicts the effect.

The STS-1 and the TCCA reference sensors provide a significant amount of coherent signal, although, not being closely collocated. The level of incoherent signal obtained by TCCA, with respect to three different pairs of TCCA reference instruments (solid, dashed, and dotted green line with filled triangles, diamonds, and squares, respectively), is at least 4 dB below the seismometer output level (solid red line, open diamonds) and the PLNM (thick solid gray line) in the entire displayed frequency band. The level is slightly below that reported by Ringler and Hutt (2010). At frequencies below 0.5 mHz, the effectiveness of the correction with the IBPM-model appears limited by the self-noise of the STS-1.

The level of noise contributed by the digitizer, as displayed in Figure 4 (dashed blue line, open downward triangle), is well

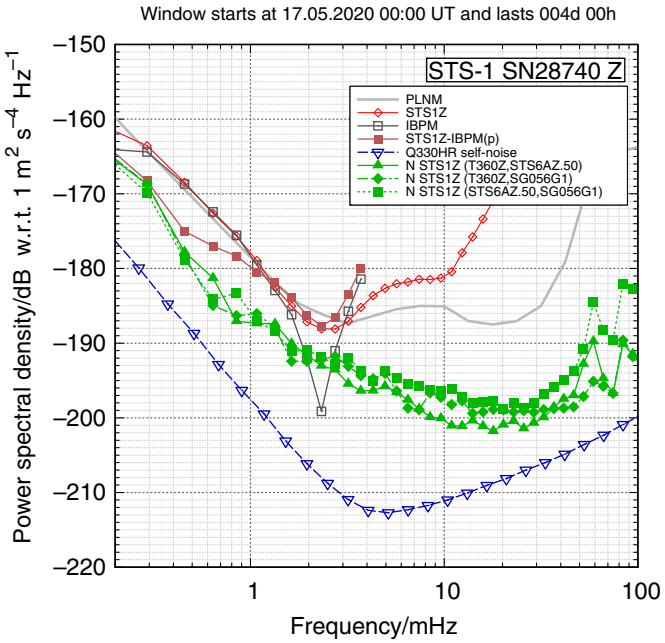

Figure 4. Analysis of the noise floor, as observed for the STS-1. The solid red line (open diamonds) gives the PSD level of the total output signal, as shown in Figure 2. The PSD of the signal contribution due to mass fluctuations in the atmosphere, as computed with the modified IBPM-model (curve IBPM), is displayed by a solid gray line (open squares). The PSD level obtained for a signal after correction with the IBPM-model is displayed by a solid dark red line (filled squares). The latter two are truncated at 4 mHz, because the signal contribution of the atmosphere is unrealistically overpredicted at higher frequency by this simple model. The dashed blue line (open downward triangle) indicates the signal contributed by the digitizer self-noise. The PSD of the incoherent signal component with respect to two TCCA reference sensors (given in parentheses in the legend) each are displayed by a solid, dashed, and dotted green line with filled triangles, diamonds, and squares, respectively. The level of the PLNM (thick solid gray line, Peterson, 1993) is displayed as a reference. The color version of this figure is available only in the electronic edition.

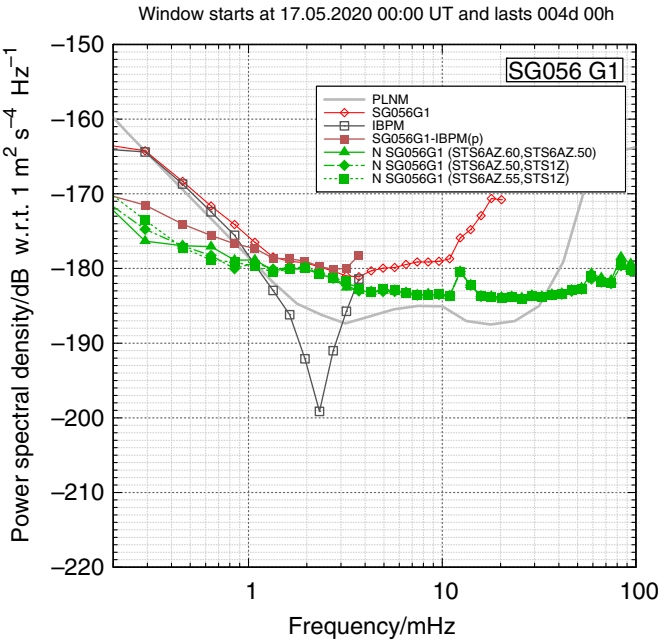

Figure 5. Analysis of the noise floor as observed for the SG056-G1. See caption of Figure 4 for details. Because of the system response of the gravimeter, the noise contributed by the digitizer lies below the displayed range. The color version of this figure is available only in the electronic edition.

below the PSD of the incoherent signal component presented in the seismometer output. Currently, it does not limit the detection level. However, if the self-noise of the sensor would be reduced by 5 dB, digitizer noise would become an issue.

The SG056-G1. A design goal of gravimeters is low drift and low noise for the observation of tidal and secular changes of gravity. The instruments are optimized for recording acceleration at ultra-low frequency. Accordingly, the output level of the SG056-G1, as displayed in Figure 5 (solid red line, open diamonds), reflects the level of the atmospherically induced signal (solid gray line, open squares) at low frequency. Moreover, the incoherent signal presented by this sensor (solid, dashed, and dotted green line with filled triangles, diamonds, and squares, respectively) is lower at the lowermost frequencies than for the STS-1, and the IBPM-correction is even more effective. However, at frequencies above 1 mHz, the SG056-G1 is limited by self-noise at a level larger than the PLNM. This limitation of SGs is well known (Rosat *et al.*, 2004). Noise levels are different for different instruments, and SG056-G1 clearly shows a smaller level of self-noise than SG056-G2 (Fig. 2). This is also reported by Rosat and Hinderer (2011) and is consistent with our result (Fig. S2). Richter *et al.* (1995) discuss thermal noise as a possible cause, which would be consistent with the heavier sensor SG056-G1 presenting a lower noise level than the lighter sensor SG056-G2. This hypothesis, however, is not yet confirmed by thorough investigation.

The level of the incoherent signal PSD is locally higher near 13 mHz (solid, dashed, and dotted green line with filled triangles, diamonds, and squares, respectively). This is a consequence of a parasitic resonance, which exists because none of the six degrees of freedom of the probe mass in the sensor is constrained by hinges or guides, as discussed by Imanishi (2009). Because the frequency response of the gravimeter is flat with respect to acceleration, and the gain of the gravimeter is adjusted to let the tidal amplitude consume the dynamic range, the contribution of digitizer noise is negligible here and offscale in Figure 5.

The STS-6A. The three sensors of type STS-6A all perform similarly well. In Figure 6, we display results for the sensor with

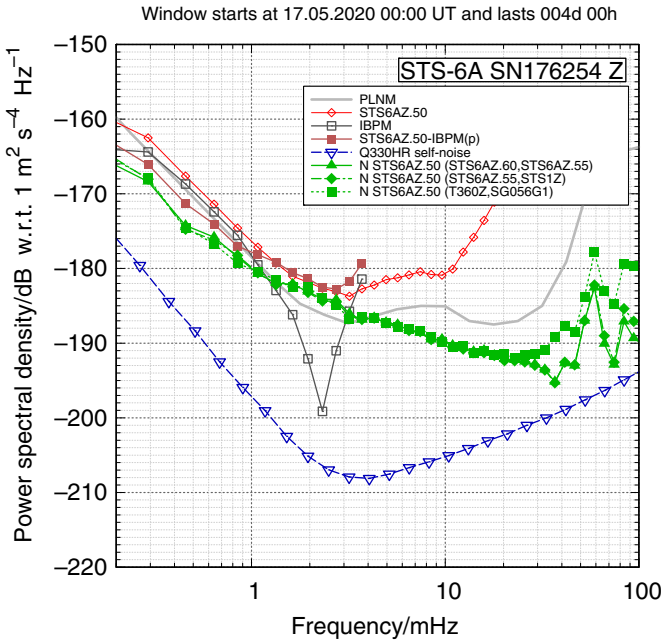

Figure 6. Analysis of the noise floor as observed for the STS-6A.50. See caption of Figure 4 for details. The color version of this figure is available only in the electronic edition.

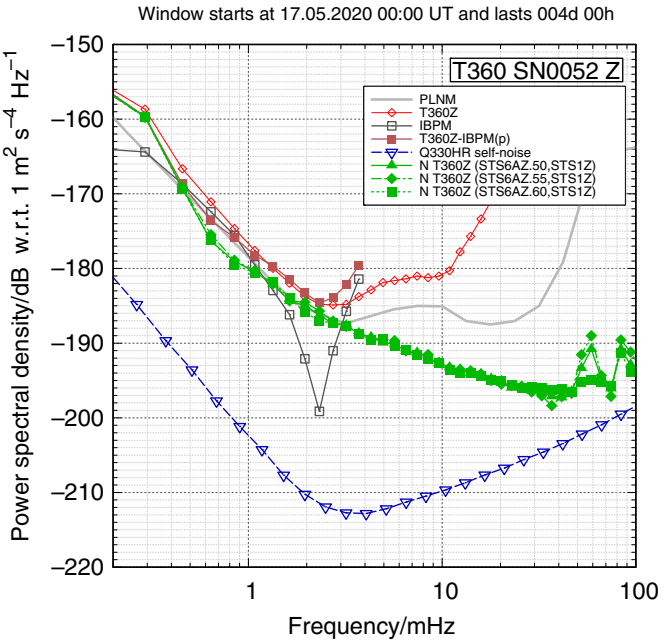

Figure 7. Analysis of the noise floor as observed for the T360. See caption of Figure 4 for details. The color version of this figure is available only in the electronic edition.

serial number SN 176254. Results for the others are provided in the Figures S3 and S4, and do not differ essentially from those presented here. Although, the PSD of the recorded signal (solid red line, open diamonds) is slightly larger than the PSD of the IBPM-model (solid gray line, open squares), the correction (solid dark red line, filled squares) still can lower the detection level below the PLNM (thick solid gray line), at frequencies below 1 mHz, though not as much as for the STS-1 (Fig. 4). Between 1.5 and 3 mHz, this sensor, however, presents a level of self-noise (solid, dashed, and dotted green line with filled triangles, diamonds, and squares, respectively) that lies above the PLNM (thick solid gray line). This elevated level appears for all three instruments and is independent of the choice of TCCA reference sensors and, hence, cannot be blamed on those.

We computed the arithmetic mean of the time-domain output signals from the vertical components of the three STS-6A (not shown in the figure). This is an acceptable test, because of the high similarity of the three sensors and their proximity to each other. The PSD of the average signal is lower than that of the individual sensor in the band from 1 to 5 mHz by a few decibels, and places the output level to between that of the T360, on the one hand, and the STS-1, on the other hand, in this band. This is a clear indication that the STS-6A is limited by incoherent self-noise in that band and not by some local disturbance, which would act coherently on each of the three sensors.

The Trillium T360. The PSD of the output of the T360 (solid red line, open diamonds), as shown in Figure 7, is slightly above the PLNM (thick solid gray line) and the PSD of the IBPM-model (solid gray line, open squares) from 0.3 to 3 mHz. The correction with the IBPM-signal does not lower the level below the PLNM. The PSD of the incoherent signal component (solid, dashed, and dotted green line with filled triangles, diamonds, and squares, respectively) hugs the PLNM between 1 and 3 mHz, and, is slightly below the PLNM, for frequencies between 0.4 and 1 mHz. At lower frequency, the instrument is limited by self-noise, with a PSD level clearly rising above the PLNM. Although, the sensor does not exceed the PLNM level with its self-noise in the normal-mode band, it does not provide a margin, which would allow to reduce the detection level below the PLNM by a correction for atmospherically induced signals.

Time-domain perspective

During a time period of several months, the T360 suffered from episodic long-period narrowband noise. Because of still unknown causes, the instrument produced oscillatory signals with a period of about 30 min to one hour, thus, compromising the observation of the lowest frequency normal modes. The STS-1 produced occasional glitches. At times, they appeared as frequently as once per day. For both of the instruments, the amplitudes of these disturbances were not larger than a few nanometers per second squared in most cases. Nevertheless, the conditions for a low detection threshold at long signal period were less fortunate for these two instruments in many time windows. Although, the origin of the problem in the T360 is still

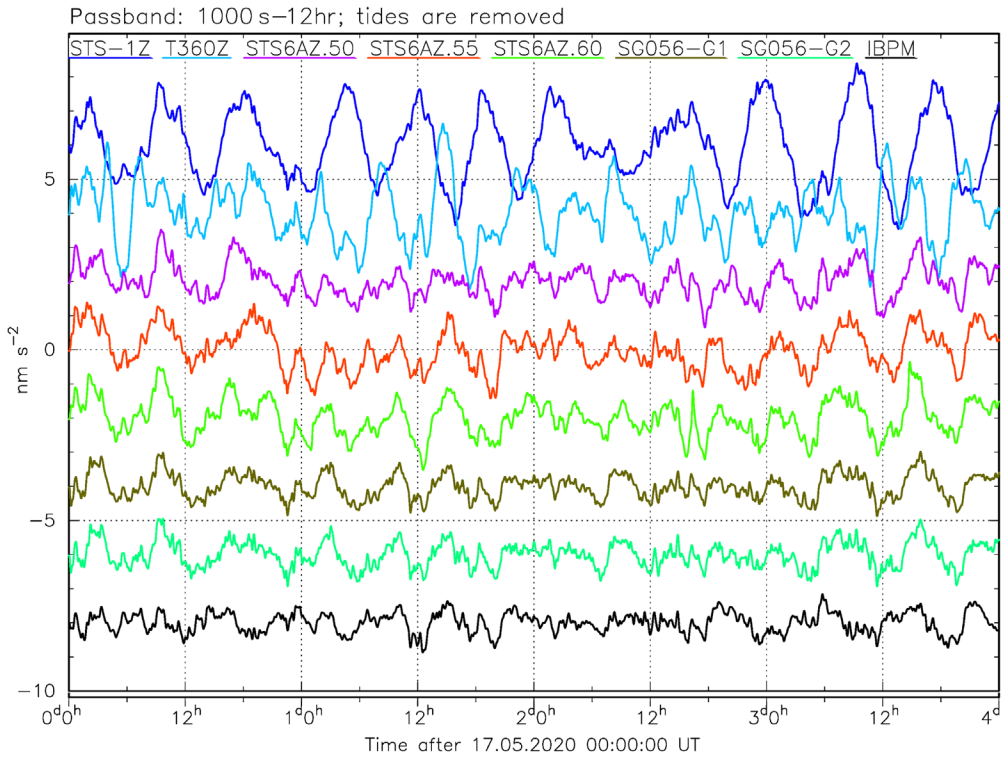

Figure 8. Seismogram comparison for signals with long signal period beyond the band analyzed in our spectral analysis. Output signals of the sensors are filtered to represent acceleration in a passband from 1000 s to 12 hr. Tidal signals are removed at frequencies of Q1, O1, K1, N2, M2, S2, and M3. No IBPM-correction is applied. The traces are offset for better comparison. Signals are (top to bottom): STS-1, T360, STS-6A.50, STS-6A.55, STS-6A.60, SG056-G1, SG056-G2, and IBPM-prediction. As always in this study, only vertical-component signals are displayed. The signal recorded by the STS-2 is not displayed. In this period range, it is dominated by self-noise at a level that would by far exceed the scale range attributed to traces in this diagram. The color version of this figure is available only in the electronic edition.

unknown, for the STS-1, the problem could be resolved by replacing the signal cable between sensor and feedback electronics. In both cases, we were unable to detect any external cause that would reliably coincide with the individual glitches or transient oscillations. The STS-6A seismometers in our installation provided a more reliable and stable signal quality.

The analysis of PSD and incoherent signal component cannot easily be extended to longer signal period within the time window of four days, as used so far. A time-domain comparison for signals filtered to represent acceleration up to 12 hr period is displayed in Figure 8. By a least-squares fit, we removed major harmonics of the tides, but applied no IBPM-correction. Although, the noise level in the signals recorded by the T360 and the STS-1 obviously increase rapidly when bandwidth is extended to lower frequency, the signal level of the STS-6A is not much larger than that of the gravimeters, and its waveform is quite similar to the waveform of gravity changes. The STS-6A demonstrates a high stability outside their natural passband (i.e., far beyond their eigenperiod of 360 s). The IBPM-model (bottom trace in Fig. 8) shows only a limited ability to predict the gravity signal, which is dominated by the effect of atmospheric mass fluctuation in this frequency band. This again indicates that the atmospheric model behind this approach is too simple. Merriam (1992) shows that, at long-signal period, the 3D nature of the mass distribution in the atmosphere must be taken into account for gravity correction.

Conclusions

In the comparison with all other instruments, the SG056-G1 presents the lowest level of self-noise at the lower margin of the investigated frequency band (i.e., 0.3 mHz), as shown in Figure 3. This, however, is clearly not the case at frequencies above 1 mHz, for which the level of self-noise of the SG056-G1 is equal or higher than that of all broadband seismometers in the comparison, except the STS-2. The broadband seismometers of type STS-1, STS-6A, and T360 resolve signals at the level of the PLNM (Peterson, 1993) throughout the normal-mode band up to 10 mHz, with one minor exception. The self-noise level of the STS-6A appears slightly larger than the PLNM between 1.5 and 3 mHz. The STS-6A, on the other hand, performed very reliable and stable over a longer period of time, producing less instrumental glitches than the STS-1 or the T360. In fact, it produced signals comparable to the gravimeter records for signal period up to 12 hr, despite the rolloff of the instruments frequency response. The STS-1 is the only sensor for which the level of self-noise is about 4 dB or more below the PLNM, for all investigated frequencies (Fig. 3).

The background signal recorded at frequencies below 3 mHz, in this study, is clearly caused by the effect of atmospheric mass fluctuation. This is the case, even though we chose a time window of exceptionally low air-pressure fluctuation. The IBPM-model proposed by Zürn and Wielandt (2007) allows us to lower the detection threshold, by applying a signal correction. The effectiveness of this correction varies, depending on the instrument and frequency band. It is limited by the self-noise of the sensors, and the signal level obtained by the correction corresponds to the incoherent signal component, as

derived by TCCA (Sleeman *et al.*, 2006). At frequencies above 1 mHz, the IBPM-model, apparently, wrongly predicts parts of the atmospherically caused signal component (which was known, when the model was invented). This suggests further improvements of respective correction procedures could be possible. One avenue that we pursue is to capture the atmospheric variations not only with one single barometer but also with a network of barometers. These data might be assimilated in time stepping simulations of the local atmosphere, to capture the 3D evolution of atmospheric mass and 2D evolution of surface pressure. The latter is not a trivial task.

Nevertheless, the current study demonstrates the potential to lower the detection limit to values below the PLNM, by an appropriate model for the signal component originating in the atmosphere. Currently, the STS-1 at BFO is the only sensor in the comparison, which could benefit from a correction throughout the entire normal-mode band, having a level of self-noise of at least 4 dB below the PLNM. It is the sensor that, most clearly shows the notch in the atmospherically induced signal near 3 mHz, in a time period of small level of fluctuation. Near the notch, all other sensors are, at least, partly limited by their self-noise. Similarly, the STS-1 is the only sensor that could contribute to the development of appropriate correction procedures at these levels, as is obvious from Figure 3.

Data and Resources

All data were recorded locally at Black Forest Observatory (1971, https://doi.org/10.5880/BFO, last accessed January 2021). Data are available from Scripps Institution Of Oceanography (1986, https://doi.org/10.7914/SN/II, last accessed January 2021) and Federal Institute for Geosciences and Natural Resources, BGR (1976, https://doi.org/10.25928/MBX6-HR74, last accessed January 2021). Data can be requested using channel codes listed in Table 1. The supplemental material for this article includes a document with additional analyses and diagrams. This is published online on the journals website. Data analysis was carried out with Seitosh (https://git.scc.kit.edu/Seitosh, last accessed January 2021). We used PGPLOT (https://sites.astro.caltech.edu/tjp/pgplot/, last accessed January 2021), gnuplot (http://www.gnuplot.info/, last accessed January 2021), and xfig (https://xfig.org/, last accessed January 2021) to prepare the figures. The article is prepared in LaTeX (http://www.tug.org/texlive/, last accessed January 2021) with support by vim (http://www.vim.org/, last accessed January 2021) and GNU make (http://www.gnu.org/software/make/make.html, last accessed January 2021). Metadata can be obtained from the Incorporated Research Institutions for Seismology MetaData Aggregator available at http://ds.iris.edu/mda/ (last accessed February 2021).

Declaration of Competing Interests

The authors acknowledge that there are no conflicts of interest recorded.

Acknowledgments

The holes for the installation of the STS-6A sensors were drilled by David Kyle Jones, Adam Ringler, Peter Duffner, and Ruedi Widmer-Schnidrig. The authors thank Peter Duffner for maintaining the Black Forest Observatory installations, with which he ensures high data quality. Adam Ringler (U.S. Geological Survey [USGS]) provided comments that helped to improve the article. Pete Davis (Incorporated Research Institutions for Seismology/Project IDA) supported this study, by providing the Trillium T360. Robert Freudenmann (Streckeisen GmbH) and Adam Ringler (USGS) supported this study, by providing seismometers of type STS-6A. The authors thank Robert Freudenmann and Sarvesh Upadhyaya (Nanometrics) for fruitful discussions of sensor design and instrument properties. The authors are grateful to Luis Rivera and an anonymous reviewer for their encouraging reviews and suggestions, which helped to improve the article. The authors thank the editor Allison Bent for supporting the article in the review process.

References

Agnew, D. C., J. Berger, W. E. Farrell, J. F. Gilbert, G. Masters, and D. Miller (1986). Project IDA: A decade in review, *EOS Trans. AGU* **67,** no. 16, 203–212, doi: 10.1029/EO067i016p00203.

Aki, K., and P. G. Richards (2002). Quantitative Seismology, Second Ed., University Science Books, Sausalito, California.

Anthony, R. E., A. T. Ringler, D. C. Wilson, M. Bahavar, and K. D. Koper (2020). How processing methodologies can distort and bias power spectral density estimates of seismic background noise, *Seismol. Res. Lett.* **91,** no. 3, 1694–1706, doi: 10.1785/0220190212.

Benioff, H., J. C. Harrison, L. LaCoste, W. H. Munk, and L. B. Slichter (1959). Searching for the Earth's free oscillations, *J. Geophys. Res.* **64,** no. 9, 1334–1337, doi: 10.1029/JZ064i009p01334.

Berger, J., P. Davis, and G. Ekström (2004). Ambient Earth noise: A survey of the global seismographic network, *J. Geophys. Res.* **109,** no. B11, online resource, B11307, doi: 10.1029/2004JB003408.

Black Forest Observatory (BFO) (1971). Black Forest Observatory data, *GFZ Data Services*, doi: 10.5880/BFO.

Blackman, R. B., and J. W. Tukey (1958). The measurement of power spectra from the point of view of communications engineering—Part I, *Bell Syst. Tech. J.* **37,** no. 1, 185–282, doi: 10.1002/j.1538-7305.1958.tb03874.x.

Busse, F. H. (1974). On the free oscillation of the Earth's inner core, *J. Geophys. Res.* **79,** no. 5, 753–757, doi: 10.1029/JB079i005p00753.

Crossley, D., J. Hinderer, and U. Riccardi (2013). The measurement of surface gravity, *Rep. Progr. Phys.* **76,** no. 4, 046101, doi: 10.1088/0034-4885/76/4/046101.

Crossley, D. J., O. G. Jensen, and J. Hinderer (1995). Effective barometric admittance and gravity residuals, *Phys. Earth Planet. In.* **90,** no. 3, 221–241, doi: 10.1016/0031-9201(95)05086-Q.

Crossley, D. J., and M. G. Rochester (1980). Simple core undertones, *Geophys. J. Int.* **60,** no. 2, 129–161, doi: 10.1111/j.1365-246X.1980.tb04287.x.

Díaz, J., M. Ruiz, J. J. Curto, J. M. Torta, J. Ledo, A. Marcuello, and P. Queralt (2020). On the observation of magnetic events on broadband seismometers, *Earth Planets Space* **72,** 109, doi: 10.1186/s40623-020-01236-9.

Duputel, Z., L. Rivera, H. Kanamori, and G. Hayes (2012). W phase source inversion for moderate to large earthquakes (1990–2010), *Geophys. J. Int.* **189,** no. 2, 1125–1147, doi: 10.1111/j.1365-246X.2012.05419.x.

Federal Institute for Geosciences and Natural Resources (BGR) (1976). German Regional Seismic Network (GRSN), doi: 10.25928/MBX6-HR74.

Forbriger, T. (2012). Recommendations for seismometer deployment and shielding, in *New Manual of Seismological Observatory Practice 2 (NMSOP2)*, P. Bormann (Editor), Second Ed., GeoForschungsZentrum, Potsdam, Germany, chap. Information Sheet 5.4, doi: 10.2312/GFZ.NMSOP-2_IS_5.4.

Forbriger, T., and A. Heck (2018). Frequency response of the superconducting gravimeter SG056, in *(Schw)Ehre, wem (Schw)Ehre gebührt: Festschrift zur Verabschiedung von Prof. Dr.-Ing. Dr. h.c. Bernhard Heck, in Schriftenreihe des Studiengangs Geodäsie und Geoinformatik/ Karlsruher Institut für Technologie, 2018 (1)*, A. Heck, K. Seitz, T. Grombein, M. Mayer, J.-M. Stövhase, H. Sumaya, M. Wampach, M. Westerhaus, L. Dalheimer, and P. Senger (Editors), KIT Scientific Publishing, Karlsruhe, Germany, 57–67, doi: 10.5445/IR/1000080212.

Forbriger, T., R. Widmer-Schnidrig, E. Wielandt, M. Hayman, and N. Ackerley (2010). Magnetic field background variations can limit the resolution of seismic broad-band sensors, *Geophys. J. Int.* **183,** 303–312, doi: 10.1111/j.1365-246X.2010.04719.x.

Gerner, A., R. Sleeman, W. Lenhardt, and B. Grasemann (2016). Improving self-noise estimates of broadband seismometers by 3D trace rotation, *Seismol. Res. Lett.* **88,** no. 1, 96–103, doi: 10.1785/0220160137.

Goodkind, J. M. (1999). The superconducting gravimeter, *Rev. Sci. Instrum.* **70,** no. 11, 4131–4151, doi: 10.1063/1.1150092.

Hafner, K., J. P. Davis, and D. C. Wilson (2018). Overview of the Global Seismographic Network (GSN), unpublished presentation at *Global Network Technical Interchange Meeting*, Institut de Physique du Globe de Paris, Paris, France, 31st January–1st February 2018.

Häfner, R., and R. Widmer-Schnidrig (2013). Signature of 3-D density structure in spectra of the spheroidal free oscillation ${}_0S_2$, *Geophys. J. Int.* **192,** no. 1, 285–294, doi: 10.1093/gji/ggs013.

Hinderer, J., D. Crossley, and R. J. Warburton (2007). Gravimetric methods—Superconducting gravity meters, in *Geodesy*, G. Schubert (Editor), Vol. 3, Treatise on Geophysics, Chap. 3.04, Elsevier B.V., Amsterdam, The Netherlands, 65–120, doi: 10.1016/B978-044452748-6.00172-3.

Houston, H. (2007). Deep earthquakes, in *Earthquake Seismology*, G. Schubert (Editor), Vol. 4, Treatise on Geophysics, Chap. 4.11, Elsevier B.V., Amsterdam, The Netherlands, 321–350, doi: 10.1016/B978-044452748-6.00071-7.

Imanishi, Y. (2009). High-frequency parasitic modes of superconducting gravimeters, *J. Geodes.* **83,** no. 5, 455–467, doi: 10.1007/s00190-008-0253-6.

Juhel, K., J.-P. Montagner, M. Vallée, J. P. Ampuero, M. Barsuglia, P. Bernard, E. Clévédé, J. Harms, and B. F. Whiting (2018). Normal mode simulation of prompt elastogravity signals induced by an earthquake rupture, *Geophys. J. Int.* **216,** no. 2, 935–947, doi: 10.1093/gji/ggy436.

Kanamori, H. (1993). W phase, *Geophys. Res. Lett.* **20,** no. 16, 1691–1694, doi: 10.1029/93GL01883.

Kanamori, H., and L. Rivera (2008). Source inversion of W phase: Speeding up seismic tsunami warning, *Geophys. J. Int.* **175,** no. 1, 222–238, doi: 10.1111/j.1365-246X.2008.03887.x.

Kinemetrics (2020). Q330HR ultra-high-resolution network-aware seismic system, datasheet, available at https://kinemetrics.com/wp-content/uploads/2017/04/datasheet-q330hr-broadband-seismic-system-quanterra.pdf (last accessed February 2021).

Kobayashi, N., and K. Nishida (1998). Continuous excitation of planetary free oscillations by atmospheric disturbances, *Nature* **395,** no. 6700, 357–360, doi: 10.1038/26427.

Kurrle, D., and R. Widmer-Schnidrig (2008). The horizontal hum of the Earth: A global background of spheroidal and toroidal modes, *Geophys. Res. Lett.* **35,** no. 6, L06304, doi: 10.1029/2007GL033125.

LaCoste, L. J. B. (1934). A new type long period seismograph, *Physics* **5,** 178–180, doi: 10.1063/1.1745248.

Laske, G., and R. Widmer-Schnidrig (2015). Theory and observations: Normal mode and surface wave observations, in *Deep Earth Seismology*, G. Schubert (Editor), Vol. 1, Treatise on Geophysics, Second Ed., chap. 1.04, Elsevier B.V., Oxford, United Kingdom, 117–167, doi: 10.1016/B978-0-444-53802-4.00003-8.

Merriam, J. B. (1992). Atmospheric pressure and gravity, *Geophys. J. Int.* **109,** no. 3, 488–500, doi: 10.1111/j.1365-246X.1992.tb00112.x.

Nawa, K., N. Suda, Y. Fukao, T. Sato, Y. Aoyama, and K. Shibuya (1998). Incessant excitation of the Earth's free oscillations, *Earth Planets Space* **50,** no. 1, 3–8, doi: 10.1186/BF03352080.

Ness, N. F., J. C. Harrison, and L. B. Slichter (1961). Observations of the free oscillations of the Earth, *J. Geophys. Res.* **66,** no. 2, 621–629, doi: 10.1029/JZ066i002p00621.

Peterson, J. (1993). Observations and modelling of background seismic noise, *U.S. Geol. Surv. Open-File Rept. 93-322*, online resource, U.S. Geological Survey, Albuquerque, New Mexico, doi: 10.3133/ofr93322.

Prothero, W. A., Jr., and J. M. Goodkind (1968). A superconducting gravimeter, *Rev. Sci. Instrum.* **39,** no. 9, 1257–1262, doi: 10.1063/1.1683645.

Richter, B., H.-G. Wenzel, W. Zürn, and F. Klopping (1995). From Chandler wobble to free oscillations: Comparison of cryogenic gravimeters and other instruments in a wide period range, *Phys. Earth Planet. In.* **91,** 131–148, doi: 10.1016/0031-9201(95)03041-T.

Ringler, A. T., and C. R. Hutt (2010). Self-noise models of seismic instruments, *Seismol. Res. Lett.* **81,** no. 6, 972–983, doi: 10.1785/gssrl.81.6.972.

Romanowicz, B., and B. Mitchell (2007). Deep Earth structure—Q of the Earth from crust to core, in *Seismology and Structure of the Earth*, G. Schubert (Editor), Vol. 1, Treatise on Geophysics, chap. 1.21, Elsevier B.V., Amsterdam, The Netherlands, 731–774, doi: 10.1016/B978-044452748-6.00024-9.

Rosat, S. (2007). Optimal seismic source mechanisms to excite the Slichter mode, in *Dynamic Planet, International Association of Geodesy Symposia*, P. Tregoning and C. Rizos (Editors), Vol. 130, Springer, Berlin, Heidelberg, doi: 10.1007/978-3-540-49350-1_83.

Rosat, S., and J. Hinderer (2011). Noise levels of superconducting gravimeters: Updated comparison and time stability, *Bull. Seismol. Soc. Am.* **101,** no. 3, 1233–1241, doi: 10.1785/0120100217.

Rosat, S., J. Hinderer, D. Crossley, and J. P. Boy (2004). Performance of superconducting gravimeters from long-period seismology to tides, *J. Geodynam.* **38,** nos. 3/5, 461–476, doi: 10.1016/j.jog.2004.07.005.

Rosat, S., J. Hinderer, D. Crossley, and L. Rivera (2003). The search for the Slichter mode: Comparison of noise levels of superconducting gravimeters and investigation of a stacking method, *Phys. Earth Planet. In.* **140,** no. 1, 183–202, doi: 10.1016/j.pepi.2003.07.010.

Rosat, S., and Y. Rogister (2012). Excitation of the Slichter mode by collision with a meteoroid or pressure variations at the surface and core boundaries, *Phys. Earth Planet. In.* **190/191,** 25–33, doi: 10.1016/j.pepi.2011.10.007.

Schaad, T. P. (2016). Nano-resolution, oceanic, atmospheric, and seismic sensors with parts-per-billion resolution, *Doc. No. G8218 Rev. F, Technical Note*, Paroscientific Inc, available at http://www.paroscientific.com/pdf/G8218_Nano-Resolution.pdf (last accessed February 2021).

Scripps Institution Of Oceanography (1986). IRIS/IDA Seismic Network, doi: 10.7914/SN/II.

Sleeman, R., A. van Wettum, and J. Trampert (2006). Three-channel correlation analysis: A new technique to measure instrumental noise of digitizers and seismic sensors, *Bull. Seismol. Soc. Am.* **96,** no. 1, 258–271, doi: 10.1785/0120050032.

Slichter, L. B. (1961a). The fundamental free mode of the Earth's inner core, *Proc. Natl. Acad. Sci. Unit. States Am.* **47,** no. 2, 186–190, doi: 10.1073/pnas.47.2.186.

Slichter, L. B. (1961b). The fundamental free mode of the Earth's inner core (erratum), *Proc. Natl. Acad. Sci. Unit. States Am.* **47,** no. 3, 416.

Smith, M. L. (1976). Translational inner core oscillations of a rotating, slightly elliptical earth, *J. Geophys. Res.* **81,** no. 17, 3055–3065, doi: 10.1029/JB081i017p03055.

Suda, N., K. Nawa, and Y. Fukao (1998). Earth's background free oscillations, *Science* **279,** no. 5359, 2089–2091, doi: 10.1126/science.279.5359.2089.

Tape, C., A. T. Ringler, and D. L. Hampton (2020). Recording the Aurora at seismometers across Alaska, *Seismol. Res. Lett.* **91,** no. 6, 3039–3053, doi: 10.1785/0220200161.

Voigt, C., C. Förste, H. Wziontek, D. Crossley, B. Meurers, V. Pálinkáš, J. Hinderer, J.-P. Boy, J.-P. Barriot, and H. Sun (2016). Report on the data base of the International Geodynamics and Earth Tide Service (IGETS), *Tech. Rept. Sci. Tech. Rept. STR – Data; 16/08*, GFZ German Research Centre for Geosciences, Potsdam, Germany, 24 pp., doi: 10.2312/GFZ.b103-16087.

Warburton, R. J., and J. M. Goodkind (1977). The influence of barometric-pressure variations on gravity, *Geophys. J. Roy. Astron. Soc.* **48,** no. 3, 281–292, doi: 10.1111/j.1365-246X.1977.tb03672.x.

Weber, J., and J. V. Larson (1966). Operation of LaCoste and Romberg gravimeter at sensitivity approaching the thermal fluctuation limits, *J. Geophys. Res.* **71,** no. 24, 6005–6009, doi: 10.1029/JZ071i024p06005.

Widmer-Schnidrig, R. (2003). What can superconducting gravimeters contribute to normal-mode seismology? *Bull. Seismol. Soc. Am.* **93,** no. 3, 1370–1380, doi: 10.1785/0120020149.

Wielandt, E. (1975). Ein astasiertes Vertikalpendel mit tragender Blattfeder, *J. Geophys.* **41,** 545–547, available at http://resolver.sub.uni-goettingen.de/purl?PPN1015067948_0041 (last accessed November 2019) (in German).

Wielandt, E. (2012). Seismic Sensors and their Calibration, in *New Manual of Seismological Observatory Practice 2 (NMSOP-2)*, P. Bormann (Editor), Chap. 5, Technical Report, GeoForschungsZentrum GFZ, Potsdam, Germany, 1–51, doi: 10.2312/GFZ.NMSOP-2_ch5.

Wielandt, E., and J. M. Steim (1986). A digital very-broad-band seismograph, *Ann. Geophys.* **4,** no. B3, 227–232, available at https://streckeisen.swiss/assets/downloads/vbb-seismograph.pdf (last accessed June 2020).

Wielandt, E., and G. Streckeisen (1982). The leaf-spring seismometer: Design and performance, *Bull. Seismol. Soc. Am.* **72,** no. 6, 2349–2367, available at http://bssa.geoscienceworld.org/content/72/6A/2349 (last accessed January 2017).

Wielandt, E., and R. Widmer-Schnidrig (2002). Seismic sensing and data acquisition in the GRSN, in *Ten Years of German Regional Seismic Network (GRSN)*, M. Korn (Editor), Wiley-VCH, Weinheim, Germany, 73–83.

Zhang, S., R. Wang, T. Dahm, S. Zhou, and S. Heimann (2020). Prompt elasto-gravity signals (PEGS) and their potential use in modern seismology, *Earth Planet. Sci. Lett.* **536,** 116150, doi: 10.1016/j.epsl.2020.116150.

Zürn, W. (2014). Listening to the Earth—The Schiltach observatory BFO, in *50 Years Geophysical Institute Karlsruhe, 1964 to 2014—Expectations and Surprises*, C. Prodehl (Editor), Geophysical Institute, Karlsruhe Institute of Technology (KIT), Karlsruhe, Germany, 285–309, doi: 10.5445/IR/1000043755.

Zürn, W., J. Exß, H. Steffen, C. Kroner, T. Jahr, and M. Westerhaus (2007). On reduction of long-period horizontal seismic noise using local barometric pressure, *Geophys. J. Int.* **171,** 780–796, doi: 10.1111/j.1365-246X.2007.03553.x.

Zürn, W., and B. Meurers (2009). Clear evidence for the sign-reversal of the pressure admittance to gravity near 3 mHz, *J. Geodynam.* **48,** 371–377.

Zürn, W., and R. Widmer (1995). On noise reduction in vertical seismic records below 2 mHz using local barometric pressure, *Geophys. Res. Lett.* **22,** no. 24, 3537–3540, doi: 10.1029/95GL03369.

Zürn, W., and E. Wielandt (2007). On the minimum of vertical seismic noise near 3 mHz, *Geophys. J. Int.* **168,** 647–658, doi: 10.1111/j.1365-246X.2006.03189.x.

Manuscript received 23 October 2020
Published online 24 March 2021